Available online at www.sciencedirect.com

ScienceDirect

Geochimica et Cosmochimica Acta 238 (2018) 438–452

Geochimica et Cosmochimica Acta

www.elsevier.com/locate/gca

# A Mesoarchean shift in uranium isotope systematics

Xiangli Wang [a,b,*], Noah J. Planavsky [c], Axel Hofmann [d], Erin E. Saupe [a,e], Brian P. De Corte [f], Pascal Philippot [g,h], Stefan V. LaLonde [i], Noah E. Jemison [j], Huijuan Zou [a], Frantz Ossa Ossa [d], Kyle Rybacki [k], Nadezhda Alfimova [l], Matthew J. Larson [f], Harilaos Tsikos [m], Philip W. Fralick [n], Thomas M. Johnson [j], Andrew C. Knudsen [f], Christopher T. Reinhard [k], Kurt O. Konhauser [o]

[a] *Department of Marine Sciences, University of South Alabama, Mobile, 36688 AL, USA*
[b] *Dauphin Island Sea Lab, Dauphin Island, 36258 AL, USA*
[c] *Department of Geology & Geophysics, Yale University, New Haven, 06511 CT, USA*
[d] *Department of Geology, University of Johannesburg, 2092 Johannesburg, South Africa*
[e] *Department of Earth Sciences, University of Oxford, S Parks Road, Oxford, UK*
[f] *Department of Geology, Lawrence University, Appleton, 54911 WI, USA*
[g] *Institut de Physique du Globe de Paris, Sorbonne-Paris Cité, Université Paris Diderot, CNRS, 1 rue Jussieu, 75238 Paris, France*
[h] *Géosciences Montpellier, CNRS-UMR 5243, Université de Montpellier, 34000 Montpellier, France*
[i] *European Institute for Marine Studies, CNRS-UMR6538 Domaines Océaniques, Technopôle Brest-Iroise, 29280 Plouzané, France*
[j] *Department of Geology, University of Illinois at Urbana-Champaign, Champaign, 61820 IL, USA*
[k] *School of Earth and Atmospheric Sciences, Georgia Institute of Technology, Atlanta, 30332 GA, USA*
[l] *St. Petersburg State University, Universitetskaya nab. 7–9, St. Petersburg 199034, Russia*
[m] *Geology Department, Rhodes University, 6140 Grahamstown, South Africa*
[n] *Department of Geology, Lakehead University, Thunder Bay, Ontario P7B 5E1, Canada*
[o] *Department of Earth & Atmospheric Sciences, University of Alberta, Edmonton, Alberta T6G 2E3, Canada*

Received 18 January 2018; accepted in revised form 15 July 2018; Available online 23 July 2018

**Abstract**

Oxygenic photosynthesis fundamentally transformed all major biogeochemical cycles and increased the size and complexity of Earth's biosphere. However, there is still debate about when this metabolism evolved. As oxygenic photosynthesis is the only significant source of $O_2$ at Earth's surface, $O_2$-sensitive trace element enrichments and isotopic signatures in Archean sedimentary rocks can potentially be used to determine the onset of oxygenic photosynthesis by tracking shifts in the oxidative capacity of Earth's surface environment. Here, we present an extensive new Archean U isotope record from iron formations, organic-rich shales, and paleosols. Variability in $\delta^{238}U$ values gradually increased from Archean to Phanerozoic, consistent with current view of gradual oxidation of Earth's surface. In addition, statistical analysis on available $\delta^{238}U$ data indicates a turning point of $\delta^{238}U$ variability at roughly 3.0 billon years ago. We suggest that such a turning point in $\delta^{238}U$ variability indicates the initiation of relatively large-scale oxidative weathering of U(IV)-bearing minerals, implying that oxygenic photosynthesis may have evolved before 3.0 billion years ago.


*Keywords:* Uranium isotope; Archean; Oxygenation; Oxygenic photosynthesis; Trace metal

* Corresponding author at: Department of Marine Sciences, University of South Alabama, Mobile, 36688 AL, USA.
*E-mail address:* xwang@southalabama.edu (X. Wang).

https://doi.org/10.1016/j.gca.2018.07.024
0016-7037/

## 1. INTRODUCTION

The emergence of oxygenic photosynthesis is a turning point in Earth's geobiological evolution. Estimates about the timing of this event range widely from the Great Oxidation Event (or GOE) at ~2.4 billion years ago (Ga) to the earliest sedimentary rocks deposited at ~3.7–3.8 Ga (Kopp et al., 2005; Holland, 2006; Anbar et al., 2007; Crowe et al., 2013; Lyons et al., 2014; Planavsky et al., 2014; Satkoski et al., 2015; Frei et al., 2016; Ward et al., 2016; Albut et al., 2018). Such large uncertainty is fueled by debate surrounding the robustness of existing records of early oxygen, such as the Archean biomarker record (French et al., 2015). Given growing concerns about biomarker fidelity, inorganic geochemical proxies have become increasingly utilized to track the evolution of biological oxygen production (Ohmoto et al., 2006; Ono et al., 2006; Anbar et al., 2007; Frei et al., 2009; Crowe et al., 2013; Planavsky et al., 2014; Satkoski et al., 2015).

Uranium isotopes (expressed as $\delta^{238}U$ relative to standard CRM112a) have been developed as a redox proxy to infer past marine redox evolution (Weyer et al., 2008; Kendall et al., 2013; Andersen et al., 2014; Dahl et al., 2014; Hinojosa et al., 2016; Lau et al., 2016; Wang et al., 2016; Andersen et al., 2017; Rolison et al., 2017). Oxidative weathering of continental rocks is the primary source of U to the oceans (Dunk et al., 2002; Tissot and Dauphas, 2015). In the modern ocean, U exists as highly soluble U (VI), with a residence time of ~500,000 years (Ku et al., 1977; Langmuir, 1978; Dunk et al., 2002). In the virtual absence of oxygen on the surface of early Earth, U would have existed exclusively as insoluble U(IV), and its transport would not have induced U isotope fractionation (Brennecka et al., 2011b; Shiel et al., 2013; Jemison et al., 2016). Only when Earth's surface oxygen levels rose above pre-biotic levels would insoluble U(IV) be oxidized to soluble U(VI) and transported to the ocean by rivers. Once U(VI) is generated, adsorption and partial reduction during transport and within ocean basins can induce large U isotope fractionations (Abe et al., 2008; Bopp et al., 2010; Brennecka et al., 2011b; Romaniello et al., 2013; Holmden et al., 2015; Noordmann et al., 2015; Stirling et al., 2015; Stylo et al., 2015; Rolison et al., 2017). Based on this framework, U isotopes have been widely utilized as a paleoredox proxy to reconstruct the oxygen evolution of the ocean (Montoya-Pino et al., 2010; Brennecka et al., 2011a; Asael et al., 2013; Kendall et al., 2013, 2015; Dahl et al., 2014; Goto et al., 2014; Lau et al., 2016; Wang et al., 2016; Bartlett et al., 2018; Clarkson et al., 2018; Wei et al., 2018; Zhang et al., 2018).

In contrast to previous studies that utilized mean sedimentary $\delta^{238}U$ to infer past marine redox state, here we focus on using the variance of $\delta^{238}U$ to track the onset of oxidation of U(IV)-bearing minerals, which in turn provides indirect evidence of the onset of oxygenic photosynthesis. Previous paleo-redox studies have found some evidence for Archean oxidative weathering in specific intervals of some sedimentary successions (Frei et al., 2009; Kendall et al., 2010; Crowe et al., 2013; Planavsky et al., 2014; Satkoski et al., 2015). Here, we report the $\delta^{238}U$ of an expansive suite of stratigraphic units deposited during Archean and Paleoproterozoic times. We then combine our data with previously published U isotope data throughout Earth's history and apply statistical approaches to identify changes in the variance of $\delta^{238}U$.

## 2. IGNEOUS BASELINE $\delta^{238}U$

Since our approach is rooted in the variability of $\delta^{238}U$, it is important to establish a baseline variability to which our $\delta^{238}U$ data can be compared. We use previously published igneous $\delta^{238}U$ data (Table S1) to represent the unfractionated continental crust (Weyer et al., 2008; Amelin et al., 2010; Brennecka, 2011; Brennecka and Wadhwa, 2012; Telus et al., 2012; Kaltenbach, 2013; Andersen et al., 2015; Goldmann et al., 2015; Tissot and Dauphas, 2015). Tissot and Dauphas (2015) calculated a narrow range of $\delta^{238}U$ for the average continental crust ($-0.29 \pm 0.03$‰) based on the proportions of different lithologies in the crust. Given that the crustal composition may have changed over time (Condie, 1993; Tang et al., 2016), we take the 95% confidence interval of available bulk igneous $\delta^{238}U$ data compiled in Tissot and Dauphas (2015) ($-0.40$‰ to $-0.17$‰, Fig. 1) as an estimate for the unfractionated continental crust, to which sedimentary rocks can be compared.

Supplementary data associated with this article can be found, in the online version, at https://doi.org/10.1016/j.gca.2018.07.024.

It is possible to fractionate $^{238}U/^{235}U$ in high-temperature processes. However, such fractionations are typically observed in extraterrestrial materials (Stirling et al., 2005; Amelin et al., 2010; Brennecka et al., 2010; Tissot et al., 2017) and some terrestrial U-bearing minerals (Hiess et al., 2012). Tissot et al. (2017) proposed that

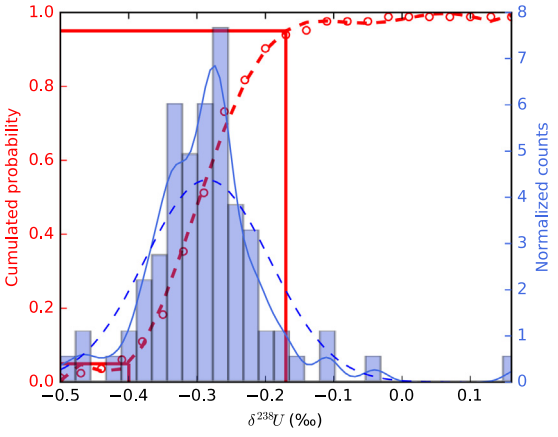


Fig. 1. Distribution of igneous $\delta^{238}U$ data. **Right axis (blue)**: normalized counts, bins = normalized histogram, blue solid line = kernel density estimation (bandwidth = 0.2), blue dashed line = idealized normal distribution using mean value of −0.285‰ and SD value of 0.09‰. **Left axis (red)**: cumulated probability, vertical red lines = 95% confidence interval (−0.40‰ to −0.17‰). (For interpretation of the references to colour in this figure legend, the reader is referred to the web version of this article.)

coordination changes involving pyroxene and olivine during early differentiation may have caused such high-temperature U isotope fractionation. Nevertheless, such anomalous U isotope fractionations are rare in bulk basaltic and granitic rocks (compiled in Tissot and Dauphas, 2015), which, together with their derived siliciclastic sediments, compose most of Earth's crust.

## 3. PRIMARY FACTOR CONTROLLING U ISOTOPE FRACTIONATION

Uranium isotope fractionation in Earth's surface environments is primarily controlled by redox reactions. Although oxidation of U(IV) to U(VI) does not fractionate $\delta^{238}U$ (Wang et al., 2015a; Andersen et al., 2016; Noordmann et al., 2016), subsequent partial reduction of U(VI) can lead to >1‰ fractionation, with $^{238}U$ enriched in U(IV) (Weyer et al., 2008; Andersen et al., 2014; Noordmann et al., 2015; Stirling et al., 2015; Stylo et al., 2015; Rolison et al., 2017). This enrichment of $^{238}U$ in U (IV) during reduction is driven by a "nuclear volume effect" (Abe et al., 2008). Laboratory experiments have demonstrated that abiotic U(VI) reduction by $S^{2-}$ and organics generally induces very small $\delta^{238}U$ fractionations, compared to microbial U(VI) reduction that consistently shows evidence for isotopically heavy U(IV) (Stylo et al., 2015). These experimental observations are consistent with observations in natural reducing marine environments (Andersen et al., 2014; Rolison et al., 2017). This implies that U(VI) reduction in marine environments is likely dominated by microbial processes. Consequently, deviation of $\delta^{238}U$ in ancient sedimentary rocks from the igneous range provides evidence for appreciable dissolved U(VI) as well as partial U(VI) reduction.

## 4. URANIUM ISOTOPE FRACTIONATION DURING SEDIMENTATION

To use sedimentary rocks to infer seawater $\delta^{238}U$ variability and thus, surface oxidative weathering, it is necessary to understand how dissolved U isotope values are transferred to sedimentary rocks.

### 4.1. Iron-rich rocks

Although ancient iron formations have not yet been applied to reconstructing seawater $\delta^{238}U$, they have been successfully used to reconstruct other marine metal records (e.g. Cr, P, REEs) due to their resistance against postdepositional alteration (Fryer, 1977; Derry and Jacobsen, 1990; Frei et al., 2009; Planavsky et al., 2010a; Planavsky et al., 2010b; Li et al., 2013; Peacock et al., 2016).

Iron formations mainly consist of iron oxides, which can sequester dissolved uranium through adsorption or reduction. Uranium(VI) adsorption onto iron oxides tends to cause small $\delta^{238}U$ fractionation (~0.2‰ or less), with $^{235}U$ being preferentially adsorbed (Weyer et al., 2008; Brennecka et al., 2011b; Shiel et al., 2013; Goto et al., 2014; Stylo et al., 2015; Jemison et al., 2016; Wang et al., 2016). Siderite and iron silicate are also major components of iron formations (Bekker et al., 2010; Rasmussen et al., 2013). These minerals likely formed during early diagenesis (Kaufman et al., 1990; Planavsky et al., 2012). Uranium (VI) reduction in ferruginous condition is still poorly understood, but existing experimental work on Fe(II) reduction of U(VI) found that $^{235}U$ is enriched in the product U (IV), contrary to biotic reduction of U(VI) (Stylo et al., 2015). Regardless of adsorptive or reductive sequestration of U into iron-rich rocks, however, generation of U isotope fractionation requires the presence of U(VI), which requires relatively high levels of oxygen.

### 4.2. Black shales

Black shales have been frequently utilized to reconstruct past seawater redox state because of their high frequency of appearance and their high abundance of redox-sensitive elements. During formation of black shales U(VI) is reduced to U(IV), with U(IV) being typically isotopically heavier (Anderson et al., 1989a, 1989b; Rolison et al., 2017), with an exception that U(VI) reduction by Fe(II) appears to generate isotopically light U(IV) (Stylo et al., 2015). The size of the effective fractionation factors has been observed to range from ~0.6‰ to ~0.8‰ (Andersen et al., 2014; Holmden et al., 2015; Noordmann et al., 2015). The observed fractionation factors are smaller than intrinsic fractionation factors predicted by nuclear volume effect and determined in experiments (Florence et al., 1975; Abe et al., 2008; Basu et al., 2014; Stirling et al., 2015; Stylo et al., 2015; Wang et al., 2015b). The discrepancy between field and laboratory observations can be attributed to a reductive-diffusive process: since U(VI) reduction typically occurs below the sediment-water interface, seawater U needs to diffuse into reducing sediments and the remaining U(VI) needs to diffuse back into the water column, and thus the overall effective isotope fractionation is dampened by this diffusional process. The net fractionation depends on the diffusional length and reaction kinetics (Clark and Johnson, 2008; Andersen et al., 2014). In addition, the effective U isotope fractionation factor may depend on many other processes such as location of reduction (within sediments vs. water column), basin restrictedness, bottom water condition, and sedimentation rates (Andersen et al., 2014; Noordmann et al., 2015; Rolison et al., 2017).

## 5. URANIUM ISOTOPE FRACTIONATION DURING WEATHERING

Paleosols have been proposed as archives for reconstructing the chemical evolution of the atmosphere (Ohmoto, 1996; Rye and Holland, 1998). Uranium can be lost to weathering fluids during granite and basalt weathering (Guthrie and Kleeman, 1986; Huang et al., 2015), or can be enriched in the residual parent rock as oxidized species during paleosol formation, likely hosted in calcite or organic matter (McCall et al., 2001). Laboratory experiments and natural observations show lack of U isotope fractionation during U loss (DeCorte et al., 2015; Huang et al., 2015; Wang et al., 2015a). However, gaining uranium during weathering may change parent rock U isotopic

composition, because the mobile U(VI) species may have experienced partial reduction and/or adsorption processes, both of which fractionate U isotopes (Bopp et al., 2009; Brennecka et al., 2011b). This gain of isotopically unconstrained U may be responsible for the fractionated U isotope compositions observed in modern soils (DeCorte et al., 2015). In summary, uranium isotopic composition in paleosols can be used to track the presence of mobile U(VI), and thus oxidative weathering.

It is important to emphasize that the exact U isotope fractionation factors during weathering, transport, and sedimentation are not critical in our approach, since it is the variance of $\delta^{238}U$, not absolute values, that are used in our approach to track the onset of oxidative mobilization of U, and by inference, oxygenic photosynthesis.

## 6. SENSITIVITY OF U(IV) OXIDATION TO ATMOSPHERIC OXYGEN

To use $\delta^{238}U$ to track biogenic oxygen level, one needs to ascertain that oxidation of U(IV) and transport of produced U(VI) to marine depositional environments requires oxygen levels significantly higher than those obtainable on a planet without oxygenic photosynthesis. To investigate the relationship between oxidation rates and surface oxygen levels, we adopted the following rate equation (Grandstaff, 1976; Ono, 2001; Johnson et al., 2014):

$$R = \frac{6.29\times10^{21}}{(RF)(10^{10.8NOC})(\rho)}\left(\sum CO_2\right)(H^+)(pO2)e^{\frac{-7045}{T}}MW_u(\mathrm{m/yr})$$

where $R$ is the radial oxidation rate (Johnson et al., 2014). RF is the retardation factor; $NOC$ is the fraction of non-uranium component in the crystal; $\Sigma CO_2$ and $H^+$ are the total dissolved carbonate and hydrogen ion concentrations in weathering fluids (Grandstaff, 1976); $pO_2$ is the atmospheric oxygen level relative to present atmospheric level, or PAL; $T$ is temperature, and $MW_u$ is the molecular weight of uraninite. Model parameters are summarized in Table S2.

Based on the above equation, the dissolution time scale of uraninite can be plotted against oxygen levels (Fig. 2). Uraninite grains with reasonable sizes will take $10^6$–$10^{10}$ years to dissolve at pre-biotic $O_2$ levels, under a wide range of other environmental conditions. The sensitivity of dissolution time scales on these parameters is generally low, and

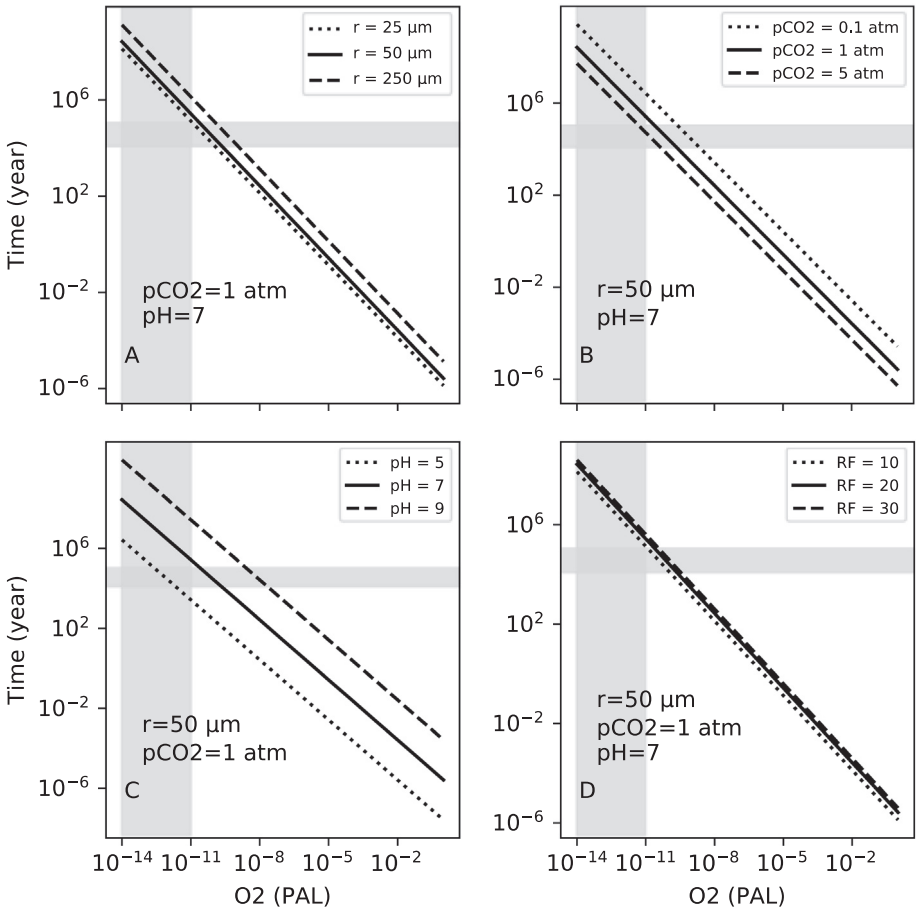


Fig. 2. Oxidative dissolution timescale of uraninite under different conditions (see text). The horizontal bars represent the upper end of typical sediment transport timescales (DePaolo et al., 2006). The vertical bars represent prebiotic oxygen levels (Haqq-Misra et al., 2011). r: radius of assumed spherical uraninite grains; RF: retardation factor.

increases in the following order: retardation factor, grain size, $pCO_2$, and $pH$. In a wide range of conditions, the dissolution timescales are generally much longer than estimated $10^4$–$10^5$ year sediment transport timescales (DePaolo et al., 2012). That a uraninite particle is unlikely to be in contact with oxygen during the full comminution timeframe makes uraninite dissolution timescale even longer. Therefore, without biological $O_2$ production, significant cycling of dissolved U(VI) in surface environments would have been unlikely. Without a mobile dissolved U (VI) pool, it is impossible to generate isotopically distinct U in ancient sedimentary environments through partial reduction or adsorption. By contrast, an active U redox cycle leads to significantly variable $\delta^{238}U$ values, as observed in modern sediments ranging from −0.9 to 0.4‰ (Andersen et al., 2014; Hinojosa et al., 2016), or even more variable in groundwater systems, ranging from ~0 to ~−3‰ (Brown et al., 2016).

## 7. SAMPLES

We report an expansive U isotope record including iron-rich rocks, organic-rich shales and paleosols to better constrain the spatiotemporal extent of oxidative weathering before the GOE. Drill core samples were preferred to minimize the possibility of supergene alteration. Tables S3 and S4 summarizes the ages, depositional environments, and metamorphic grades of all rock units investigated in this study. Sample descriptions are provided in the Supplementary data.

## 8. METHODS

For black shales, powders were ashed at 550 °C for 24 hours to destroy organic matter. Ashed shale powders and paleosols were then completely dissolved in mixed $HNO_3$ (15 N) and HF (29 N) acids on a hotplate. We used 1 mL HF and 0.2 mL $HNO_3$ for every 100 mg powder. After heating at 130 °C for 2–4 days, samples were dried down at 100 °C on hotplates. To dissolve fluorides, the samples were repeatedly refluxed with 6 N HCl (dry-down in between, 15 mL 6 N HCl for 1 g sample powder). For iron-rich and carbonate samples, powders were first treated with 6 N HCl to dissolve iron oxides and carbonates, respectively, then the residual silicates, if any, were dissolved by the aforementioned HF-$HNO_3$-HCl procedures.

We also used an acid leaching procedure to isolate authigenic (i.e. hydrogenous) U from detrital U in black shales. We gauge if our leaching technique generated an isotopic fractionation by leaching the same sample with different strengths of acid: 0.5 N $HNO_3$, 2 N $HNO_3$, and 7 N $HNO_3$, which resulted the same $\delta^{238}U$ (Table S8). 2 N $HNO_3$ was chosen as the leaching acid.

U concentrations of dissolved samples were measured on a Thermo Scientific Element XR ICP-MS. Proper amounts of $^{233}U$-$^{236}U$ double spike (see Wang et al., 2016 and references therein) were mixed and equilibrated with digested sample solutions (in 6 N HCl). Spiked samples were passed through a UTEVA ion exchange procedure to extract U from the matrix (Weyer et al., 2008). Uranium isotope ratios were measured on a Thermo Neptune Plus MC-ICP-MS. The instrument was operated at 1100 W plasma power and was set at low mass resolution ($M/\Delta M \approx 500$). $N_2$ was used to stabilize the signal. The sample introduction system comprises a 50 μL/min PFA μFlow nebulizer (Elemental Scientific), Apex IR, a Jet sampler cone, and an H skimmer cone. With this configuration, 50–60 volt $^{238}U$ was achieved on a $10^{11}$ Ω resistor with a 50 ppb U solution.

Given the large contrast between $^{238}U$ and other U isotopes, we corrected the tailing of $^{238}U$ onto adjacent peaks. Specifically, signals were measured at half masses below and above the nominal masses for 30 s, and then subtracted from on-peak signals (Hiess et al., 2012). Thorium was monitored and shown to be at very low levels ($^{232}Th/^{233}U < 10^{-2}$) due to effective ion exchange separation and, therefore, ThH hydride correction was not performed. Tail-corrected $^{233}U/^{236}U$ was used to calculate mass bias using the exponential law (Taylor et al., 1995), which was then used to extract sample $^{238}U/^{235}U$.

Amplifier gain factors were measured before each session. $^{234}U$ was measured with a $10^{12}$ Ω resistor while other isotopes ($^{232}Th$, $^{233}U$, $^{236}U$, $^{238}U$) were measured with $10^{11}$ Ω resistors. One measurement comprised 5 blocks of 10 cycles, with each cycle lasting 4.19 s. Every three samples were bracketed by spiked CRM 112a (New Brunswick Laboratory, U.S. DOE) standard solution with a similar concentration as samples. During this project, the long-term reproducibility of CRM 112a measurement was 0.02 ± 0.07‰ (2SD, n = 223). Sample values were normalized to the bracketing CRM112a during each analytical session, with errors propagated using 2SD of CRM112 in that session, which is typically smaller than the long-term 0.07‰ due to differing day-to-day instrument tuning.

The total procedure blank (digestion and column chemistry) ranged from 20 to 60 pg, which was negligible compared to 50–100 ng samples (<0.1%). Therefore, blank correction was not performed because the correction is smaller than the instrument counting error. To assess reproducibility of the method, we routinely processed various geological reference materials through the digestion and column chemistry. We also routinely analyzed unprocessed secondary standard solutions, with CRM129a = −1.70 ± 0.02‰ (Brunswick Laboratory, U.S. DOE), IRMM REIMEP 18a = −0.16 ± 0.02‰ (JRC, Brussels, Belgium), BHVO-2 = −0.24 ± 0.02‰ (USGS), Nod-a-1 = −0.59 ± 0.03‰ (USGS), and BCR = −0.26 ± 0.03‰ (USGS). The results of these standards agree well with previous studies (Table S5). The external precision for $\delta^{238}U$ measurement is 0.07‰, the largest 2 SDs of various measured geological reference materials and bracketing CRM 112a measured throughout the projects.

## 9. RESULTS

Our $\delta^{238}U$ new data (Tables S6–8), combined with published data (Table S9), exhibit an overall trend of increasing variability through time (Fig. 3A). Black shale $\delta^{238}U$ values were largely within the igneous range before 2.4 Ga, but

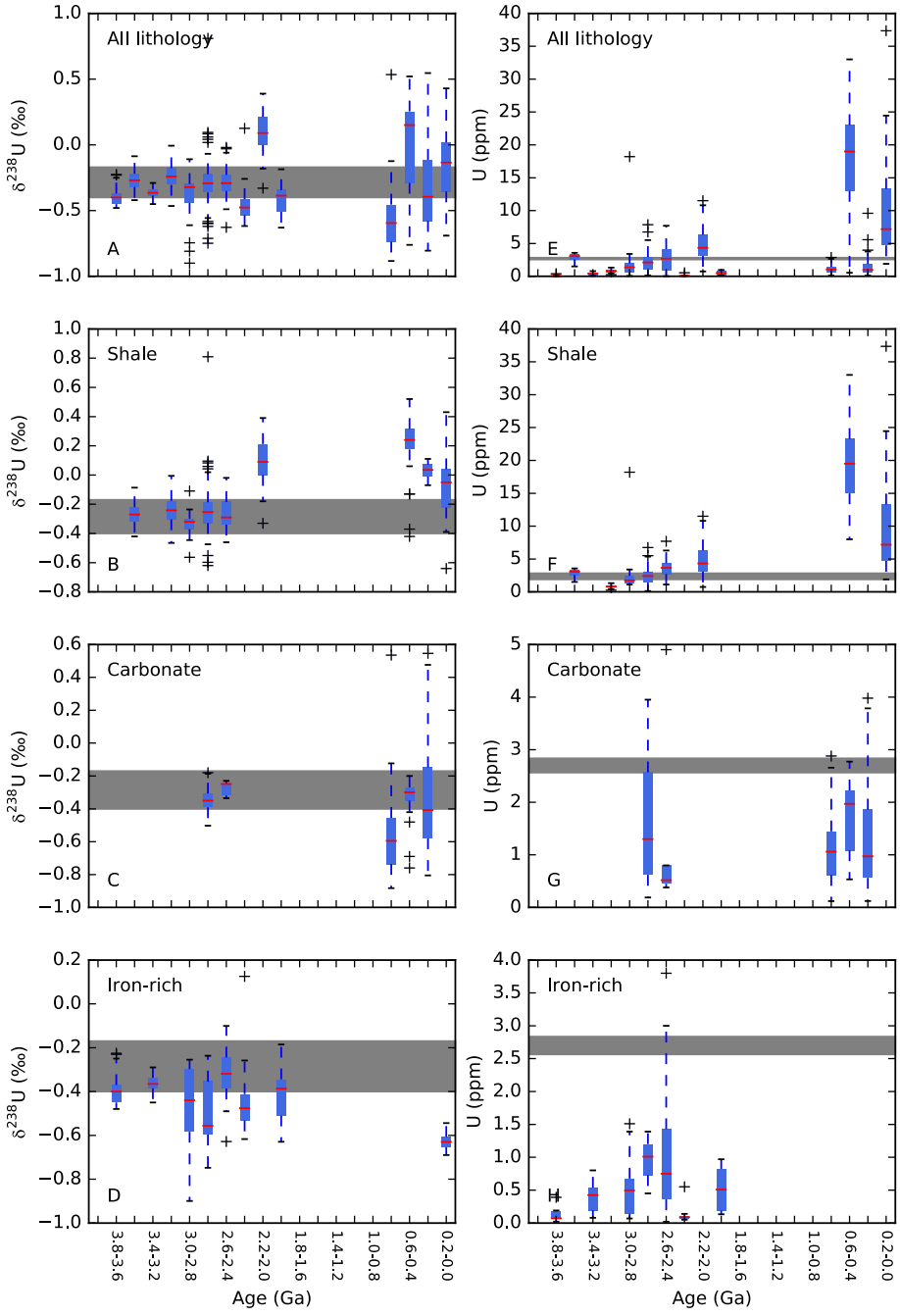


Fig. 3. Boxplots for $\delta^{238}U$ and U concentrations binned into 200 million year time windows, with all lithologies plotted together in A and E, and individually in other subplots. The red line in each box represents the mean of that time window. The horizontal bars in A–D represent the $\delta^{238}U$ of igneous rocks. The horizontal line in E–H represents the U concentration (2.6–2.8 ppm) of the upper continental crust (Condie, 1993).

increased above the igneous range after 2.4 Ga (Fig. 3B). Iron formation and published carbonate data are largely within or below the igneous range (Fig. 3C and D). U concentration data show similar patterns (Fig. 3E–H). Paleosol samples (2.2 Ga–3.0 Ga) are plotted in Fig. 4A, which shows fractionated values both above (up to 0.1‰) and below (down to −0.8‰) the igneous range. There is a weak correlation between U and Th ($r^2 = 0.580$, $p < 0.0001$, Fig. 4B), and the slope in the U-Th space is slightly steeper than that of the average continental crust (Rudnick and Gao, 2003). No correlation between $\delta^{238}U$ and U/Th was observed.

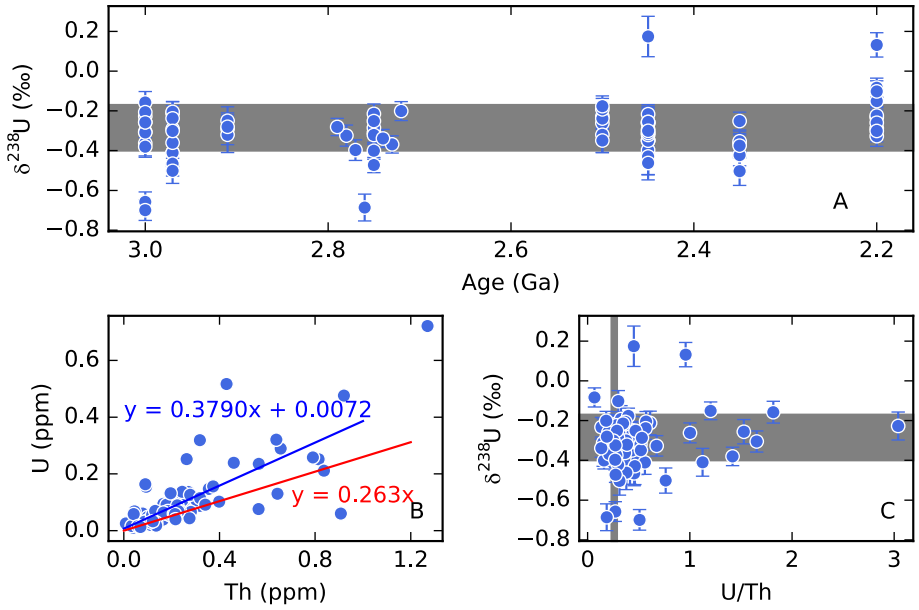


Fig. 4. Results for paleosols. The horizontal gray bars in A and C represent the igneous $\delta^{238}U$. The vertical gray bar in C represent the U/Th in the upper continental crust (Rudnick and Gao, 2003). The red line in B represents the expected relationship between U and Th in the UCC (Rudnick and Gao, 2003), whereas the blue line is a least square linear regression of data ($r^2 = 0.580$, $p < 0.0001$). (For interpretation of the references to colour in this figure legend, the reader is referred to the web version of this article.)

## 10. DISCUSSION

### 10.1. Temporal increase in the variability of sedimentary $\delta^{238}U$

To quantitatively evaluate how $\delta^{238}U$ and its variability have evolved over geological time, we binned the $\delta^{238}U$ data into 200 Myr time windows. Then the standard deviation (SD) is calculated for each time window through 1000 bootstrapping replicates. When different lithologies are combined, the bootstrapped SD shows an increasing trend (Fig. 5c), consistent with the general view that Earth's oxidation is a protracted process. The SD is below that of published igneous rocks before ~3.0 Ga, and shifts to above igneous after ~3.0 Ga. Similarly, the mean $\delta^{238}U$ values of time bins before 3.0 Ga are within the UCC range, whereas those after 3.0 Ga are mainly distributed below the UCC range, with one exception between 2.4 Ga and 2.6 Ga (Fig. 3D). Importantly, the lack of $\delta^{238}U$ fractionation in pre-3.0 Ga rocks (and many post-3.0 Ga ones) suggests that background processes (e.g., lightning-generated minor oxidants such as nitrate and hydrogen peroxide (Hazen et al., 2009; Ettwig et al., 2010) do not substantially mobilize uranium.

Two lines of reasoning support our approach of evaluating the $\delta^{238}U$ variability on combined lithologies. First, combined lithology leads to larger sample number in each time bin and, thus, a more robust statistic framework. Second, this approach does not inherently produce false positives. Although different lithologies will have different $\delta^{238}U$ values even when they precipitate from the same seawater due to different fractionation mechanisms, such lithological offset can only occur under an oxic world when U (VI) is present. Therefore, combining different lithologies would not generate ostensibly enhanced $\delta^{238}U$ variance if there were no oxidative U mobilization (i.e., 'false positives'). However, we also plotted the data of individual lithologies, with the same overall trend observed in each sedimentary archive, albeit with some exceptions (Fig. S1).

A shift in $\delta^{238}U$ variability at or before ~3.0 Ga is compatible with earlier findings from other isotope systems about biogenic oxygen production in the Mesoarchean (Planavsky et al., 2014; Satkoski et al., 2015). On an early Earth, biogenic oxygen production would have occurred under a generally reducing atmosphere. Therefore, oxygen distribution on early Earth was likely highly heterogeneous and dynamic (fluctuating spatiotemporally). Therefore, some "oxygen oases" may have existed before Earth's surface was widely oxygenated enough to generate U isotope fractionation with statistical significance.

### 10.2. Change point test for $\delta^{238}U$ variability

To pinpoint the turning point in the history of $\delta^{238}U$ variability from a statistical perspective, we used a likelihood-based framework to independently identify changes in $\delta^{238}U$ variance through time (Killick and Eckley, 2014). The *cpt.var* function in the R package *changepoint* was used to statistically assess significant changes in variance (note that no change will be found if variance structure remains constant throughout a data series). The *cpt.varmean* and *cpt.mean* functions were used to search for significant change points in variance + mean and mean, respectively. We searched for multiple breaks in variance using both an assumed distribution and a distribution-free method for our test statistic, with the mean

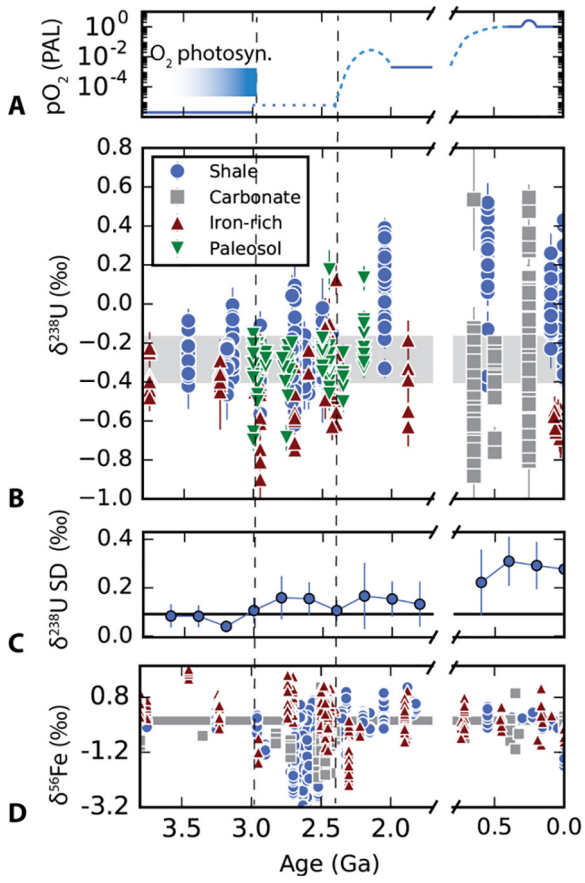


Fig. 5. Compiled geochemical records. A, a view of oxygen evolution; B, the U isotope record from this study and previous studies (n = 933, this study n = 372), with the horizontal bar representing the $\delta^{238}U$ range for igneous rocks (see SI); C, SD of the U isotope record, with each point representing 200-Myr data, with the horizontal line denoting the SD of $\delta^{238}U$ in igneous rocks; D, previous iron isotope record (n = 1445) (Rouxel et al., 2005; Planavsky et al., 2012; Li et al., 2013; Satkoski et al., 2015), with the horizontal bar representing the −0.1–+0.1‰ range for igneous rocks), same legend as in B. Vertical dashed lines represent 2.95 Ga and 2.43 Ga identified by change point tests.

estimated via maximum likelihood. Both methods returned equivalent results and, thus, we present only those for the normal test statistic.

For all lithologies or for iron rich-rocks considered alone, the CPT returns the same earliest break point in $\delta^{238}U$ variance at 2.95 Ga (Fig. 6 A and B, respectively). The CPT result for shales (2.43 Ga, Fig. 6C) postdates that for iron-rich rocks. We attribute this offset in timing to varying detrital influences in these lithologies. Specifically, iron-rich rocks precipitate directly from seawater and have minimal detrital contributions. In contrast, U in shales includes both authigenic and detrital components, with the former being sourced from seawater (Andersen et al., 2014; Rolison et al., 2017). If dissolved U is very low, the authigenic signal would be muted by the unfractionated detrital component (see below for acid leaching test). This provides a plausible scenario for the unfractionated $\delta^{238}U$ (Fig. 3B) and low U/Th in black shales deposited before 2.4 Ga (Partin et al., 2013). Combining observations based on CPT tests for iron formations and shales, we suggest that dissolved U(VI) was present in seawater at small concentrations between ~3.0 Ga and ~2.4 Ga, and significantly increased after 2.4 Ga.

### 10.3. $\delta^{238}U$ in iron formations

The statistical finding of the turning point in $\delta^{238}U$ variability at 2.95 Ga depends on the iron-rich samples from the Sinqeni Formation. Therefore, it is critical to consider the preservation of these rocks. We did not conduct new petrographic work on these samples given previous reflected light microscopy, backscatter electron microscopy, and laser ablation work. Specifically, abundant reduced Mn and Fe mineral phases in Sinqeni iron formations suggest that these rocks have not been subject to postdepositional supergene alteration (Planavsky et al., 2014; Albut et al., 2018).

The lack of $\delta^{238}U$ variability in pre-3.0 Ga iron formation samples suggests minimal presence of dissolved U (VI) in rivers and seawater. It also suggests that ferric iron in terrestrial and marine sediments–for instance, generated by photochemical reactions (Konhauser et al., 2007)–does not lead to U oxidation and $\delta^{238}U$ variability. In contrast, samples deposited after 3.0 Ga vary widely, mostly below the igneous range and, thus, consistent with adsorption of dissolved U(VI) to oxides. Alternatively, the light $\delta^{238}U$ values could be tied to reduction of U(VI) by Fe(II) (Stylo et al., 2015). Either way, fractionation of $\delta^{238}U$ in iron formations will require appreciable dissolved U(VI) that requires relatively high level of oxygen. Three samples (GL56 299.23 from the 2.4 Ga Hotazel Formation, and DGM3/B and DGM6/B from the 2.48 Ga Dales Gorge Formation) have positive $\delta^{238}U$ values relative to igneous rocks. These three samples have lower U concentrations (<70 ppb) than other iron-rich samples and can be explained by trapping the small amount of residual, isotopically heavy U(VI) at the end stage of reduction by Fe(II) (Stylo et al., 2015). Nevertheless, removing these three anomalous samples does not alter the statistical results.

### 10.4. $\delta^{238}U$ in black shales

Unlike iron formations, where U is almost exclusively derived from seawater, black shale U is a mixture of seawater-derived (authigenic) and detrital U. The black shale U concentrations vary widely (Fig. 3F), reflecting different extents of authigenic U enrichment. Most pre-2.95 Ga samples fall into this category. With very low oxygen on Earth's surface, there would be limited dissolved U (VI) and low U enrichments. Such low dissolved U(VI), when sequestered in black shales, can easily be overwhelmed by unfractionated detrital U. This can be illustrated by comparing $\delta^{238}U$ in the iron-rich rocks from the Sinqeni Formation and shales from the Ntombe Formation, both of which belong to the Pongola Supergroup and were deposited at approximately the same time. The light values in the Sinqeni iron-rich rocks likely reflect partial adsorption or partial reduction by Fe(II) of the low

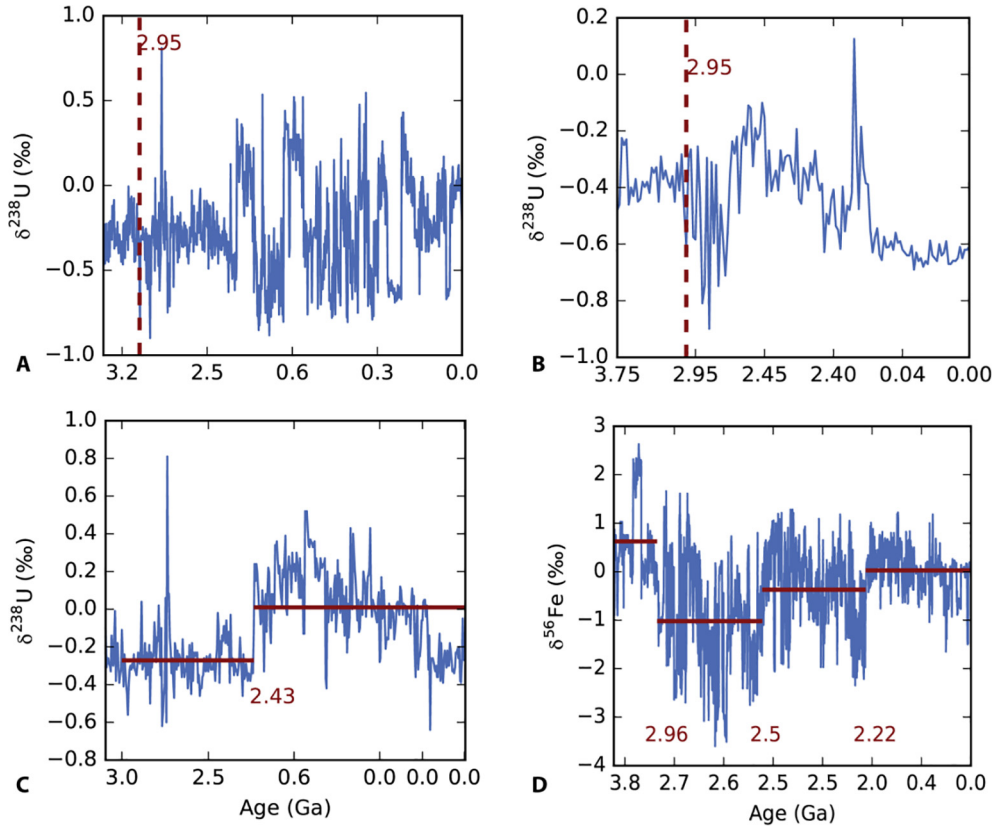


Fig. 6. Results of change-point tests for different lithologies. A, $\delta^{238}U$ in all lithologies (break point in variance); B, $\delta^{238}U$ in iron-rich rocks (break point in variance); C, $\delta^{238}U$ in black shales (break point in mean + variance); D, previously published $\delta^{56}Fe$ record (break points in variance + mean).

level U(VI) dissolved in seawater, but such low level of U would not be enough to escape the overwhelming signal from detrital U in black shales in the Ntombe Formation. When oxygen increased at a later time, however, more U (VI) can be generated and delivered to the ocean, leading to higher authigenic U enrichment and positive $\delta^{238}U$ values (after 2.4 Ga, Fig. 3B and F).

To test the hypothesis that the lack of fractionated $\delta^{238}U$ between 2.95 Ga and 2.43 Ga is due to domination of detrital U over authigenic U, in the late stage of this project we conducted acid leaching experiment on a suit of ca. 2.7 Ga organic-rich shales from Abitibi Greenstone Belt. Using 2 N $HNO_3$ leaching, we observed fractionated authigenic U in the Abitibi shales (Table S8). This confirms that dissolved U(VI) existed at 2.7 Ga, but was too small to generate enough authigenic U in shale to compete against the effect of unfractionated detrital U, leading to muted bulk shale $\delta^{238}U$ values. Future studies should focus on the authigenic U in more Archean black shales and compare with our $\delta^{238}U$ record in iron-rich rocks.

There is a positive linear relationship between $\delta^{238}U$ and [U] ($r^2 = 0.351$, $p < 0.0001$, Fig. 7A, notice the log scale on the x-axis). However, the linear relationship is weaker if $\delta^{238}U$ is plotted against U/Al ($r^2 = 0.11$, $p < 0.00001$, Fig. 7B). Aluminum, like Th, is considered as solely sourced from detrital materials and it has little ability to move during diagenesis. Therefore, normalizing metal concentrations to Al concentration can remove U concentration variation due to dilutions by carbonate, opal, or detrital materials (Brumsack, 1989; Calvert and Pedersen, 1993; Morford and Emerson, 1999; Piper and Perkins, 2004; Tribovillard et al., 2006). The triangular shape of the fractionated samples in the $\delta^{238}U$-U/Al plot (Fig. 7B) can be explained by the diffusive-reactive process, which has previously been described in detail (Clark and Johnson, 2008; Andersen et al., 2014; Rolison et al., 2017). Briefly, as seawater U (VI) diffuses down across the sediment-water interface, partial reduction pushes the remaining U(VI) in porewater to lower $\delta^{238}U$. At certain depth below the SWI, porewater dissolved U(VI) would become undetectable (Olson et al., 2017). The $\delta^{238}U$ values of the reduced U(IV) near the SWI would be positive, offset from seawater by a positive fractionation factor of roughly 0.6‰ (Andersen et al., 2014), although this value could be smaller or even negative if Fe(II) is present (Stylo et al., 2015). Uranium(IV) produced in deeper sediments would be lighter (potentially negative). As sediments are buried deeper and receive more later-stage U from porewater, the isotopically light U could become dominant, until the sediments are buried below the point where no new U(IV) is produced. Taken together, these processes could lead to the triangular shape of the fractionated shales shown in Fig. 3B.

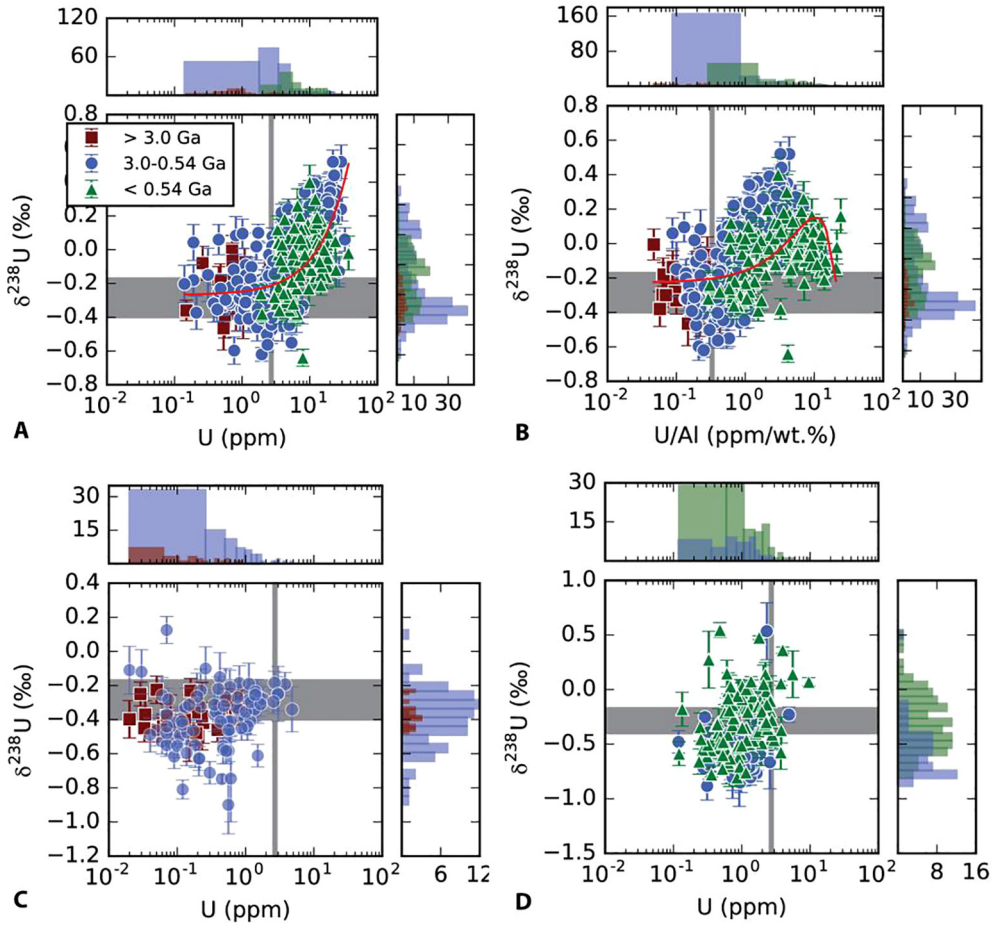


Fig. 7. Cross-plots between $\delta^{238}U$ and U enrichment, with corresponding histograms for $\delta^{238}U$ and U distributions. A–B, shales; C, iron-rich rocks; D, carbonates. The red line in A is a linear fit to all $\delta^{238}U$-[U] data except samples with [U] > 60 ppm (deemed as outliers for this plot only) ($r^2 = 0.35$, $p < 0.00001$, more in SI). The red line in B is a second order polynomial fit to all $\delta^{238}U$ and U/Al data ($r^2 = 0.23$, $p < 0.00001$, more in SI). The horizontal bars in all figures represent the $\delta^{238}U$ range of igneous rocks (Tissot and Dauphas, 2015) (Fig. 1). The vertical bars in A–D represent the U concentration or the U/Al ratio of the average upper continental crust (Rudnick and Gao, 2003).

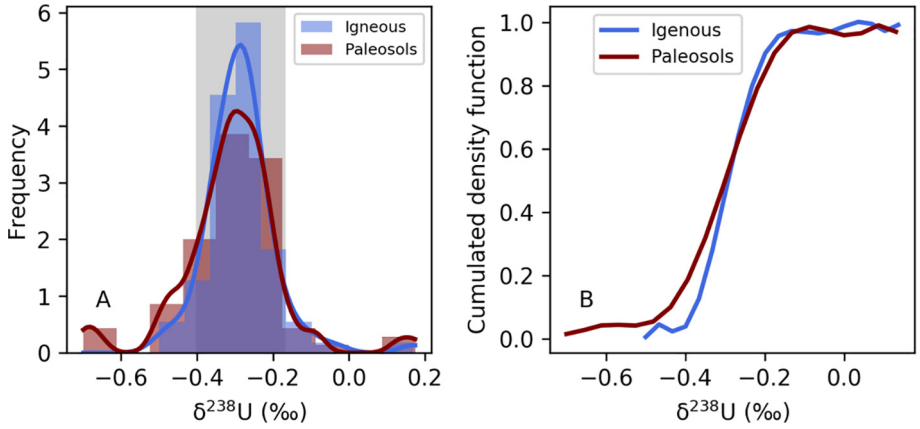


Fig. 8. Comparison of $\delta^{238}U$ values between igneous rocks and paleosols investigated in this study. A: histograms with corresponding Gaussian Kernel Density Estimations; the vertical bar shows the 95% level of unfractionated BSE (Fig. 1). B: cumulated probability of $\delta^{238}U$ values.

### 10.5. $\delta^{238}U$ in paleosols

Compared to igneous rocks, the paleosol samples have slightly more variable and more negative $\delta^{238}U$ values (Fig. 8). About 10% of the paleosol samples are fractionated, which is comparable to modern soils (DeCorte et al., 2015). Although the average $\delta^{238}U$ of paleosol samples overlap with igneous data, paleosols have slightly wider spread, especially for lower $\delta^{238}U$ values (Fig. 8).

Although weathering does not generate a significant U isotope fractionation (Wang et al., 2015a; Andersen et al., 2016), fractionated $\delta^{238}U$ values in soils may be due to receiving U(VI) through adsorption, receiving U(IV) through partial reduction of U(VI) carried in weathering fluids, or inheriting parent sedimentary rocks with fractionated $\delta^{238}U$ values. Some of our paleosol samples have fractionated $\delta^{238}U$ and high U/Th ratios, relative to the UCC (Fig. 4C). Since the parent rocks of our paleosol samples are igneous rocks, the starting $\delta^{238}U$ should be close to the UCC (−0.17‰ to −0.40‰). Therefore, samples with positively fractionated $\delta^{238}U$ can be attributed to capturing U(IV) through reduction, and samples with negatively fractionated $\delta^{238}U$ can be attributed to capturing U(VI) through adsorption.

### 10.6. Reconciling U isotope data with the sulfur MIF record

Our U isotope evidence of early oxygenation is compatible with the mass-independent sulfur isotope record. Archean $pO_2$ was thought to be low ($<10^{-7} - 10^{-5}$ PAL) before the GOE (~2.4 Ga), based on mass-independent S isotope (MIF-S) signatures in sedimentary rocks (Farquhar and Wing, 2005; Zahnle et al., 2006). Even at $10^{-7} - 10^{-5}$ PAL $pO_2$ levels, U(IV) oxidation would be limited but still present (Fig. 2), at least sporadically if not pervasively. Further, not all pre-2.4 Ga rocks have MIF-S signals, suggesting that oxygen levels likely fluctuated dramatically during the Archean Era (Ohmoto et al., 2006; Ono et al., 2006). With a small $O_2$ reservoir, atmospheric oxygen levels were likely highly dynamic, with oxygen concentrations varying significantly on short time scales. Uranium oxidation could have occurred during short-lived excursions to higher atmospheric oxygen levels in an overall low-oxygen Earth system. This dynamic oxygenation hypothesis is consistent with our observed oscillation in the SD of $\delta^{238}U$ throughout Archean (Fig. 5C). Moreover, U oxidation could also have occurred within locally oxygenated microenvironments. For instance, microbial mats in shallow marine or lacustrine settings have been suggested to host locally high-$O_2$ environments conducive to oxidative weathering of substrate rocks, even under an anoxic atmosphere (Lalonde and Konhauser, 2015).

### 10.7. Coupling with the iron isotope record

Existing iron isotope records are consistent with a significant shift in the oxidative capacity of Earth's surface around 3.0 Ga (Fig. 5D). The most pronounced shift in sedimentary Fe isotope values occur at ~3.0 Ga, determined using the same statistical change point test we used to track shifts in U cycling (Fig. 6D). Iron isotope values in iron-rich rocks prior to 3.0 Ga are generally positive, which is most likely due to minor Fe(II) oxidation by anoxygenic photosynthesis or photochemical oxidation (Konhauser et al., 2002; Rouxel et al., 2005; Johnson et al., 2008; Satkoski et al., 2015). After 3.0 Ga, however, sedimentary iron isotope values are highly variable, including strong negative $\delta^{56}Fe$ values. This increase in iron isotope variability is more likely explained by extensive water column oxygen production and intense microbial iron cycling (Rouxel et al., 2005; Planavsky et al., 2012; Busigny et al., 2014), consistent with our U isotope records.

## 11. CONCLUDING REMARKS

Uranium isotope records in black shales, iron formations, and paleosols, together with iron isotopes in iron formations suggest that biogenic oxygen production on Earth likely started at least 3.0 billion years ago, consistent with previous conclusions based on other redox-sensitive proxies (Crowe et al., 2013; Planavsky et al., 2014; Satkoski et al., 2015) and some phylogenic predictions (David and Alm, 2011; Dvořák et al., 2014). Given an early rise in oxygenic photosynthesis, the protracted oxygenation of Earth's surface was likely linked to other factors such as continental emergence, shifting crustal composition from mafic to felsic, or the drawdown of large masses of reducing gases and minerals required to enable the later rise of atmospheric $O_2$ at the GOE (Zahnle et al., 2006; Campbell and Allen, 2008; Lalonde and Konhauser, 2015; Smit and Mezger, 2017).

## ACKNOWLEDGEMENTS

This research was supported by Agouron Institute Postdoctoral Fellowship Program, the UnivEarths Labex Programme at Sorbonne Paris Cité (ANR-10-LABX-0023 and ANR-11-IDEX-0005-02) and the São Paulo Research Foundation (FAPESP, grant 2015/16235-2) and the NASA Astrobiology Institute under CooperativeAgreement No. NNA15BB03A issued through the Science Mission Directorate.

## REFERENCES

Abe M., Suzuki T., Fujii Y., Hada M. and Hirao K. (2008) An ab initio molecular orbital study of the nuclear volume effects in uranium isotope fractionations. *J. Chem. Phys.* **129**, 164309.

Albut G., Babechuk M. G., Kleinhanns I. C., Benger M., Beukes N. J., Steinhilber B., Smith A. J., Kruger S. J. and Schoenberg R. (2018) Modern rather than Mesoarchaean oxidative weathering responsible for the heavy stable Cr isotopic signatures of the 2.95 Ga old Ijzermijn iron formation (South Africa). *Geochim. Cosmochim. Acta* **228**, 157–189.

Amelin Y., Kaltenbach A., Iizuka T., Stirling C. H., Ireland T. R., Petaev M. and Jacobsen S. B. (2010) U-Pb chronology of the solar system's oldest solids with variable $^{238}U/^{235}U$. *Earth. Planet. Sci. Lett.* **300**, 343–350.

Anbar A. D., Duan Y., Lyons T. W., Arnold G. L., Kendall B., Creaser R. A., Kaufman A. J., Gordon G. W., Scott C. and Garvin J. (2007) A whiff of oxygen before the great oxidation event? *Science* **317**, 1903–1906.

Andersen M. B., Elliott T., Freymuth H., Sims K. W., Niu Y. and Kelley K. A. (2015) The terrestrial uranium isotope cycle. *Nature* **517**, 356–359.

Andersen M. B., Romaniello S., Vance D., Little S. H., Herdman R. and Lyons T. W. (2014) A modern framework for the interpretation of $^{238}U/^{235}U$ in studies of ancient ocean redox. *Earth. Planet. Sci. Lett.* **400**, 184–194.

Andersen M. B., Stirling C. H. and Weyer S. (2017) Uranium isotope fractionation. *Rev. Mineral. Geochem.* **82**, 799–850.

Andersen M. B., Vance D., Morford J. L., Bura-Nakić E., Breitenbach S. F. M. and Och L. (2016) Closing in on the marine $^{238}U/^{235}U$ budget. *Chem. Geol.* **420**, 11–22.

Anderson R., LeHuray A., Fleisher M. and Murray J. (1989a) Uranium deposition in Saanich Inlet sediments, Vancouver Island. *Geochim. Cosmochim. Acta* **53**, 2205–2213.

Anderson R. F., Fleisher M. Q. and LeHuray A. P. (1989b) Concentration, oxidation state, and particulate flux of uranium in the Black Sea. *Geochim. Cosmochim. Acta* **53**, 2215–2224.

Asael D., Tissot F. L., Reinhard C. T., Rouxel O., Dauphas N., Lyons T. W., Ponzevera E., Liorzou C. and Chéron S. (2013) Coupled molybdenum, iron and uranium stable isotopes as oceanic paleoredox proxies during the Paleoproterozoic Shunga Event. *Chem. Geol.* **362**, 193–210.

Bartlett R., Elrick M., Wheeley J. R., Polyak V., Desrochers A. and Asmerom Y. (2018) Abrupt global-ocean anoxia during the Late Ordovician–early Silurian detected using uranium isotopes of marine carbonates. *Proc. Natl. Acad. Sci.*, 201802438.

Basu A., Sanford R. A., Johnson T. M., Lundstrom C. C. and Löfler F. E. (2014) Uranium isotopic fractionation factors during U(VI) reduction by bacterial isolates. *Geochim. Cosmochim. Acta* **136**, 100–113.

Bekker A., Slack J. F., Planavsky N., Krapež B., Hofmann A., Konhauser K. O. and Rouxel O. J. (2010) Iron formation: the sedimentary product of a complex interplay among mantle, tectonic, oceanic, and biospheric processes. *Econ. Geol.* **105**, 467–508.

Bopp C. J., Lundstrom C. C., Johnson T. M. and Glessner J. J. G. (2009) Variations in $^{238}U/^{235}U$ in uranium ore deposits: isotopic signatures of the U reduction process? *Geology* **37**, 611–614.

Bopp C. J., Lundstrom C. C., Johnson T. M., Sanford R. A., Long P. E. and Williams K. H. (2010) Uranium $^{238}U/^{235}U$ isotope ratios as indicators of reduction: results from an in situ biostimulation experiment at Rifle, Colorado, USA. *Environ. Sci. Technol.* **44**, 5927–5933.

Brennecka G., Weyer S., Wadhwa M., Janney P., Zipfel J. and Anbar A. (2010) 238U/235U variations in meteorites: extant 247Cm and implications for Pb-Pb dating. *Science* **327**, 449–451.

Brennecka G. A. (2011) *Uranium Isotope Variations in Nature: Mechanisms, Applications, and Implications* Ph.D. thesis. Arizona State University.

Brennecka G. A., Herrmann A. D., Algeo T. J. and Anbar A. D. (2011a) Rapid expansion of oceanic anoxia immediately before the end-Permian mass extinction. *Proc. Natl. Acad. Sci.* **108**, 17631–17634.

Brennecka G. A. and Wadhwa M. (2012) Uranium isotope compositions of the basaltic angrite meteorites and the chronological implications for the early Solar System. *Proc. Natl. Acad. Sci.* **109**, 9299–9303.

Brennecka G. A., Wasylenki L. E., Bargar J. R., Weyer S. and Anbar A. D. (2011b) Uranium isotope fractionation during adsorption to Mn-oxyhydroxides. *Environ. Sci. Technol.* **45**, 1370–1375.

Brown S. T., Basu A., Christensen J. N., Reimus P., Heikoop J., Simmons A., WoldeGabriel G., Maher K., Weaver K. and Clay J. (2016) Isotopic evidence for reductive immobilization of uranium across a roll-front mineral deposit. *Environ. Sci. Technol.* **50**, 6189–6198.

Brumsack H.-J. (1989) Geochemistry of recent TOC-rich sediments from the Gulf of California and the Black Sea. *Geologische Rundschau* **78**, 851–882.

Busigny V., Planavsky N. J., Jézéquel D., Crowe S., Louvat P., Moureau J., Viollier E. and Lyons T. W. (2014) Iron isotopes in an Archean ocean analogue. *Geochim. Cosmochim. Acta* **133**, 443–462.

Calvert S. and Pedersen T. (1993) Geochemistry of recent oxic and anoxic marine sediments: implications for the geological record. *Mar. Geol.* **113**, 67–88.

Campbell I. H. and Allen C. M. (2008) Formation of supercontinents linked to increases in atmospheric oxygen. *Nat. Geosci.* **1**, 554–558.

Clark S. K. and Johnson T. M. (2008) Effective isotopic fractionation factors for solute removal by reactive sediments: a laboratory microcosm and slurry study. *Environ. Sci. Technol.* **42**, 7850–7855.

Clarkson M. O., Stirling C. H., Jenkyns H. C., Dickson A. J., Porcelli D., Moy C. M., von Strandmann P. A. P., Cooke I. R. and Lenton T. M. (2018) Uranium isotope evidence for two episodes of deoxygenation during Oceanic Anoxic Event 2. *Proc. Natl. Acad. Sci.*, 201715278.

Condie K. C. (1993) Chemical composition and evolution of the upper continental crust: contrasting results from surface samples and shales. *Chem. Geol.* **104**, 1–37.

Crowe S. A., Døssing L. N., Beukes N. J., Bau M., Kruger S. J., Frei R. and Canfield D. E. (2013) Atmospheric oxygenation three billion years ago. *Nature* **501**, 535–538.

Dahl T. W., Boyle R. A., Canfield D. E., Connelly J. N., Gill B. C., Lenton T. M. and Bizzarro M. (2014) Uranium isotopes distinguish two geochemically distinct stages during the later Cambrian SPICE event. *Earth. Planet. Sci. Lett.* **401**, 313–326.

David L. A. and Alm E. J. (2011) Rapid evolutionary innovation during an Archaean genetic expansion. *Nature* **469**, 93–96.

DeCorte B., Planavsky N., Wang X. L., Auerbach D. J. and Knudsen A. (2015) Uranium Isotope Ratios in Modern and Precambrian Soils. AGU Fall Meeting. San Francisco CA. #PP31B-2235 (abstr.).

DePaolo D. J., Lee V. E., Christensen J. N. and Maher K. (2012) Uranium comminution ages: Sediment transport and deposition time scales. *Comptes Rendus Geosci.* **344**, 678–687.

DePaolo D. J., Maher K., Christensen J. N. and McManus J. (2006) Sediment transport time measured with U-series isotopes: results from ODP North Atlantic drift site 984. *Earth. Planet. Sci. Lett.* **248**, 394–410.

Derry L. A. and Jacobsen S. B. (1990) The chemical evolution of Precambrian seawater: evidence from REEs in banded iron formations. *Geochim. Cosmochim. Acta* **54**, 2965–2977.

Dunk R., Mills R. and Jenkins W. (2002) A reevaluation of the oceanic uranium budget for the Holocene. *Chem. Geol.* **190**, 45–67.

Dvořák P., Casamatta D. A., Poulíčková A., Hašler P., Ondřej V. and Sanges R. (2014) Synechococcus: 3 billion years of global dominance. *Mol. Ecol.* **23**, 5538–5551.

Ettwig K. F., Butler M. K., Le Paslier D., Pelletier E., Mangenot S., Kuypers M. M., Schreiber F., Dutilh B. E., Zedelius J. and De Beer D. (2010) Nitrite-driven anaerobic methane oxidation by oxygenic bacteria. *Nature* **464**, 543–548.

Farquhar J. and Wing B. A. (2005) The terrestrial record of stable sulphur isotopes: a review of the implications for evolution of Earth's sulphur cycle. *Geol. Soc. Spec. Publ.* **248**, 167–177.

Florence T., Batley G., Ekstrom A., Fardy J. and Farrar Y. (1975) Separation of uranium isotopes by Uranium(IV)-Uranium(VI) chemical exchange. *J. Inorg. Nucl. Chem.* **37**, 1961–1966.

Frei R., Gaucher C., Poulton S. W. and Canfield D. E. (2009) Fluctuations in Precambrian atmospheric oxygenation recorded by chromium isotopes. *Nature* **461**, 250–253.

Frei R., Crowe S. A., Bau M., Polat A., Fowle D. A. and Døssing L. N. (2016) Oxidative elemental cycling under the low O2 Eoarchean atmosphere. *Sci. Rep.* **6**, 1–9.

French K. L., Hallmann C., Hope J. M., Schoon P. L., Zumberge J. A., Hoshino Y., Peters C. A., George S. C., Love G. D. and Brocks J. J. (2015) Reappraisal of hydrocarbon biomarkers in Archean rocks. *Proc. Natl. Acad. Sci.* **112**, 5915–5920.

Fryer B. (1977) Rare earth evidence in iron-formations for changing Precambrian oxidation states. *Geochim. Cosmochim. Acta* **41**, 361–367.

Goldmann A., Brennecka G., Noordmann J., Weyer S. and Wadhwa M. (2015) The uranium isotopic composition of the earth and the solar system. *Geochim. Cosmochim. Acta* **148**, 145–158.

Goto K. T., Anbar A. D., Gordon G. W., Romaniello S. J., Shimoda G., Takaya Y., Tokumaru A., Nozaki T., Suzuki K., Machida S., Hanyu T. and Usui A. (2014) Uranium isotope systematics of ferromanganese crusts in the Pacific Ocean: implications for the marine $^{238}U/^{235}U$ isotope system. *Geochim. Cosmochim. Acta* **146**, 43–58.

Grandstaff D. (1976) A kinetic study of the dissolution of uraninite. *Econ. Geol.* **71**, 1493–1506.

Guthrie V. and Kleeman J. (1986) Changing uranium distributions during weathering of granite. *Chem. Geol.* **54**, 113–126.

Haqq-Misra J., Kasting J. F. and Lee S. (2011) Availability of $O_2$ and $H_2O_2$ on pre-photosynthetic earth. *Astrobiology* **11**, 293–302.

Hazen R. M., Ewing R. C. and Sverjensky D. A. (2009) Evolution of uranium and thorium minerals. *Am. Mineral.* **94**, 1293–1311.

Hiess J., Condon D. J., McLean N. and Noble S. R. (2012) 238U/235U systematics in terrestrial uranium-bearing minerals. *Science* **335**, 1610–1614.

Hinojosa J. L., Stirling C. H., Reid M. R., Moy C. M. and Wilson G. S. (2016) Trace metal cycling and 238 U/235 U in New Zealand's fjords: implications for reconstructing global paleo-redox conditions in organic-rich sediments. *Geochim. Cosmochim. Acta* **179**, 89–109.

Holland H. D. (2006) The oxygenation of the atmosphere and oceans. *Philos Trans. Roy. Soc. Lond. B Biol. Sci.* **361**, 903–915.

Holmden C., Amini M. and Francois R. (2015) Uranium isotope fractionation in Saanich Inlet: a modern analog study of a paleoredox tracer. *Geochim. Cosmochim. Acta* **153**, 202–215.

Huang J., Zhou Z., Gong Y., Lundstrom C. and Huang F. (2015) Uranium isotope composition of a laterite profile during extreme weathering of basalt in Guangdong, South China. AGU Fall Meeting Abstracts. (abstr.).

Jemison N. E., Johnson T. M., Shiel A. and Lundstrom C. (2016) Uranium isotopic fractionation induced by U (VI) adsorption onto common aquifer minerals. *Environ. Sci. Technol.* **50**, 12232–12240.

Johnson C. M., Beard B. L. and Roden E. E. (2008) The iron isotope fingerprints of redox and biogeochemical cycling in modern and ancient Earth. *Annu. Rev. Earth Planet. Sci.* **36**, 457–493.

Johnson J. E., Gerpheide A., Lamb M. P. and Fischer W. W. (2014) $O_2$ constraints from Paleoproterozoic detrital pyrite and uraninite. *Geol. Soc. Am. Bull.* **B30949**, 30941.

Kaltenbach A. (2013) *Uranium Isotopic Analysis of Terrestrial and Extraterrestrial Samples*. University of Otago.

Kaufman A. J., Hayes J. and Klein C. (1990) Primary and diagenetic controls of isotopic compositions of iron-formation carbonates. *Geochim. Cosmochim. Acta* **54**, 3461–3473.

Kendall B., Brennecka G. A., Weyer S. and Anbar A. D. (2013) Uranium isotope fractionation suggests oxidative uranium mobilization at 2.50 Ga. *Chem. Geol.* **362**, 105–114.

Kendall B., Komiya T., Lyons T. W., Bates S. M., Gordon G. W., Romaniello S. J., Jiang G., Creaser R. A., Xiao S. and McFadden K. (2015) Uranium and molybdenum isotope evidence for an episode of widespread ocean oxygenation during the late Ediacaran Period. *Geochim. Cosmochim. Acta* **156**, 173–193.

Kendall B., Reinhard C. T., Lyons T. W., Kaufman A. J., Poulton S. W. and Anbar A. D. (2010) Pervasive oxygenation along late Archaean ocean margins. *Nat. Geosci.* **3**, 647–652.

Killick R. and Eckley I. (2014) changepoint: an R package for changepoint analysis. *J. Stat. Softw.* **58**, 1–19.

Konhauser K. O., Hamade T., Raiswell R., Morris R. C., Ferris F. G., Southam G. and Canfield D. E. (2002) Could bacteria have formed the Precambrian banded iron formations? *Geology* **30**, 1079–1082.

Konhauser K. O., Amskold L., Lalonde S. V., Posth N. R., Kappler A. and Anbar A. (2007) Decoupling photochemical Fe (II) oxidation from shallow-water BIF deposition. *Earth. Planet. Sci. Lett.* **258**, 87–100.

Kopp R. E., Kirschvink J. L., Hilburn I. A. and Nash C. Z. (2005) The Paleoproterozoic snowball Earth: a climate disaster triggered by the evolution of oxygenic photosynthesis. *Proc. Natl. Acad. Sci.* **102**, 11131–11136.

Ku T.-L., Knauss K. G. and Mathieu G. G. (1977) Uranium in open ocean: concentration and isotopic composition. *Deep Sea Res.* **24**, 1005–1017.

Lalonde S. V. and Konhauser K. O. (2015) Benthic perspective on Earth's oldest evidence for oxygenic photosynthesis. *Proc. Natl. Acad. Sci.* **112**, 995–1000.

Langmuir D. (1978) Uranium solution-mineral equilibria at low temperatures with applications to sedimentary ore deposits. *Geochim. Cosmochim. Acta* **42**, 547–569.

Lau K. V., Maher K., Altiner D., Kelley B. M., Kump L. R., Lehrmann D. J., Silva-Tamayo J. C., Weaver K. L., Yu M. and Payne J. L. (2016) Marine anoxia and delayed Earth system recovery after the end-Permian extinction. *Proc. Natl. Acad. Sci.* **113**, 2360–2365.

Li W., Czaja A. D., Van Kranendonk M. J., Beard B. L., Roden E. E. and Johnson C. M. (2013) An anoxic, Fe (II)-rich, U-poor ocean 3.46 billion years ago. *Geochim. Cosmochim. Acta* **120**, 65–79.

Lyons T. W., Reinhard C. T. and Planavsky N. J. (2014) The rise of oxygen in Earth's early ocean and atmosphere. *Nature* **506**, 307–315.

McCall K., Lanzirotti A. and Rasbury E. (2001) Uranium (VI) incorporation in paleosol calcite: evidence for sequestration of U on geologic time scales. *Natl. Synchrotron Light Source Activity Rep. Sci. Highlights* **2001**, 2–93.

Montoya-Pino C., Weyer S., Anbar A. D., Pross J., Oschmann W., van de Schootbrugge B. and Arz H. W. (2010) Global enhancement of ocean anoxia during Oceanic Anoxic Event 2: a quantitative approach using U isotopes. *Geology* **38**, 315–318.

Morford J. L. and Emerson S. (1999) The geochemistry of redox sensitive trace metals in sediments. *Geochim. Cosmochim. Acta* **63**, 1735–1750.

Noordmann J., Weyer S., Montoya-Pino C., Dellwig O., Neubert N., Eckert S., Paetzel M. and Böttcher M. (2015) Uranium and molybdenum isotope systematics in modern euxinic basins: case studies from the central Baltic Sea and the Kyllaren fjord (Norway). *Chem. Geol.* **396**, 182–195.

Noordmann J., Weyer S., Georg R. B., Jöns S. and Sharma M. (2016) 238U/235U isotope ratios of crustal material, rivers and products of hydrothermal alteration: new insights on the oceanic U isotope mass balance. *Isotopes. Environ. Health. Stud.* **52**, 141–163.

Ohmoto H. (1996) Evidence in pre–2.2 Ga paleosols for the early evolution of atmospheric oxygen and terrestrial biota. *Geology* **24**, 1135–1138.

Ohmoto H., Watanabe Y., Ikemi H., Poulson S. R. and Taylor B. E. (2006) Sulphur isotope evidence for an oxic Archaean atmosphere. *Nature* **442**, 908–911.

Olson L., Quinn K. A., Siebecker M. G., Luther G. W., Hastings D. and Morford J. L. (2017) Trace metal diagenesis in sulfidic sediments: Insights from Chesapeake Bay. *Chem. Geol.*.

Ono S. (2001) *Detrital Uraninite and the Early Earth's Atmosphere: SIMS Analyses of Uraninite in the Elliot Lake District and the Dissolution Kinetics of Natural Uraninite* Ph.D thesis. Pennsylvania State University.

Ono S., Beukes N. J., Rumble D. and Fogel M. L. (2006) Early evolution of atmospheric oxygen from multiple-sulfur and carbon isotope records of the 2.9 Ga Mozaan Group of the Pongola Supergroup, Southern Africa. *S. Afr. J. Geol.* **109**, 97–108.

Partin C., Bekker A., Planavsky N., Scott C., Gill B., Li C., Podkovyrov V., Maslov A., Konhauser K. and Lalonde S. (2013) Large-scale fluctuations in Precambrian atmospheric and oceanic oxygen levels from the record of U in shales. *Earth. Planet. Sci. Lett.* **369–370**, 284–293.

Peacock C. L., Lalonde S. V. and Konhauser K. O. (2016) Iron minerals as archives of Earth's redox and biogeochemical evolution. *EMU Notes Mineral.* **17**, 113–164.

Piper D. and Perkins R. (2004) A modern vs. Permian black shale—the hydrography, primary productivity, and water-column chemistry of deposition. *Chem. Geol.* **206**, 177–197.

Planavsky N., Bekker A., Rouxel O. J., Kamber B., Hofmann A., Knudsen A. and Lyons T. W. (2010a) Rare Earth Element and yttrium compositions of Archean and Paleoproterozoic Fe formations revisited: New perspectives on the significance and mechanisms of deposition. *Geochim. Cosmochim. Acta* **74**, 6387–6405.

Planavsky N. J., Rouxel O. J., Bekker A., Lalonde S. V., Konhauser K. O., Reinhard C. T. and Lyons T. W. (2010b) The evolution of the marine phosphate reservoir. *Nature* **467**, 1088–1090.

Planavsky N., Rouxel O. J., Bekker A., Hofmann A., Little C. T. and Lyons T. W. (2012) Iron isotope composition of some Archean and Proterozoic iron formations. *Geochim. Cosmochim. Acta* **80**, 158–169.

Planavsky N. J., Asael D., Hofmann A., Reinhard C. T., Lalonde S. V., Knudsen A., Wang X. L., Ossa F. O., Pecoits E., Smith A. J. B., Beukes N. J., Bekker A., Johnson T. M., Konhauser K. O., Lyons T. W. and Rouxel O. J. (2014) Evidence for oxygenic photosynthesis half a billion years before the Great Oxidation Event. *Nat. Geosci.* **7**, 283–286.

Rasmussen B., Meier D. B., Krapež B. and Muhling J. R. (2013) Iron silicate microgranules as precursor sediments to 2.5-billion-year-old banded iron formations. *Geology* **41**, 435–438.

Rolison J. M., Stirling C. H., Middag R. and Rijkenberg M. J. (2017) Uranium stable isotope fractionation in the Black Sea: modern calibration of the 238 U/235 U paleo-redox proxy. *Geochim. Cosmochim. Acta* **203**, 69–88.

Romaniello S. J., Herrmann A. D. and Anbar A. D. (2013) Uranium concentrations and 238U/235U isotope ratios in modern carbonates from the Bahamas: Assessing a novel paleoredox proxy. *Chem. Geol.* **362**, 305–316.

Rouxel O. J., Bekker A. and Edwards K. J. (2005) Iron isotope constraints on the Archean and Paleoproterozoic ocean redox state. *Science* **307**, 1088–1091.

Rudnick R. L. and Gao S. (2003) Composition of the Continental Crust. In *Treatise on Geochemistry* (eds. K. Turekian and H. D. Holland). Pergamon, Oxford, pp. 1–64.

Rye R. and Holland H. D. (1998) Paleosols and the evolution of atmospheric oxygen: a critical review. *Am. J. Sci.* **298**, 621–672.

Satkoski A. M., Beukes N. J., Li W., Beard B. L. and Johnson C. M. (2015) A redox-stratified ocean 3.2 billion years ago. *Earth. Planet. Sci. Lett.* **430**, 43–53.

Shiel A. E., Laubach P. G., Johnson T. M., Lundstrom C. C., Long P. E. and Williams K. H. (2013) No measurable changes in 238U/235U due to desorption-adsorption of U(VI) from groundwater at the Rifle, Colorado, Integrated Field Research Challenge Site. *Environ. Sci. Technol.* **47**, 2535–2541.

Smit M. A. and Mezger K. (2017) Earth's early O2 cycle suppressed by primitive continents. *Nat. Geosci.*.

Stirling C., Halliday A. and Porcelli D. (2005) In search of live $^{247}$Cm in the early solar system. *Geochim. Cosmochim. Acta* **69**, 1059–1071.

Stirling C. H., Andersen M. B., Warthmann R. and Halliday A. N. (2015) Isotope fractionation of 238U and 235U during biologically-mediated uranium reduction. *Geochim. Cosmochim. Acta* **163**, 200–218.

Stylo M., Neubert N., Wang Y., Monga N., Romaniello S. J., Weyer S. and Bernier-Latmani R. (2015) Uranium isotopes fingerprint biotic reduction. *Proc. Natl. Acad. Sci.* **112**, 5619–5624.

Tang M., Chen K. and Rudnick R. L. (2016) Archean upper crust transition from mafic to felsic marks the onset of plate tectonics. *Science* **351**, 372–375.

Taylor P. D., de Bièvre P., Walder A. J. and Entwistle A. (1995) Validation of the analytical linearity and mass discrimination correction model exhibited by a multiple collector inductively coupled plasma mass spectrometer by means of a set of synthetic uranium isotope mixtures. *J. Anal. At. Spectrom.* **10**, 395–398.

Telus M., Dauphas N., Moynier F., Tissot F. c. F. L., Teng F.-Z., Nabelek P. I., Craddock P. R. and Groat L. A. (2012) Iron, zinc, magnesium and uranium isotopic fractionation during continental crust differentiation: the tale from migmatites, granitoids, and pegmatites. *Geochim. Cosmochim. Acta* **97**, 247–265.

Tissot F. L. and Dauphas N. (2015) Uranium isotopic compositions of the crust and ocean: Age corrections, U budget and global extent of modern anoxia. *Geochim. Cosmochim. Acta* **167**, 113–143.

Tissot F. L., Dauphas N. and Grove T. L. (2017) Distinct 238U/235U ratios and REE patterns in plutonic and volcanic angrites: geochronologic implications and evidence for U isotope fractionation during magmatic processes. *Geochim. Cosmochim. Acta* **213**, 593–617.

Tribovillard N., Algeo T. J., Lyons T. and Riboulleau A. (2006) Trace metals as paleoredox and paleoproductivity proxies: an update. *Chem. Geol.* **232**, 12–32.

Wang X. L., Johnson T. M. and Lundstrom C. C. (2015a) Isotope fractionation during oxidation of tetravalent uranium by dissolved oxygen. *Geochim. Cosmochim. Acta* **150**, 160–170.

Wang X. L., Johnson T. M. and Lundstrom C. C. (2015b) Low temperature equilibrium isotope fractionation and isotope exchange kinetics between U (IV) and U (VI). *Geochim. Cosmochim. Acta* **158**, 262–275.

Wang X. L., Planavsky N., Reinhard C., Hein J. R. and Johnson T. M. (2016) A Cenozoic seawater redox record derived from $^{238}$U/$^{235}$U in ferromanganese crusts. *Am. J. Sci.* **316**, 64–83.

Ward L. M., Kirschvink J. L. and Fischer W. W. (2016) Timescales of oxygenation following the evolution of oxygenic photosynthesis. *Orig. Life. Evol. Biosph.* **46**, 51–65.

Wei G.-Y., Planavsky N. J., Tarhan L. G., Chen X., Wei W., Li D. and Ling H.-F. (2018) Marine redox fluctuation as a potential trigger for the Cambrian explosion. *Geology*.

Weyer S., Anbar A., Gerdes A., Gordon G., Algeo T. and Boyle E. (2008) Natural fractionation of 238U/235U. *Geochim. Cosmochim. Acta* **72**, 345–359.

Zahnle K., Claire M. and Catling D. (2006) The loss of mass-independent fractionation in sulfur due to a Palaeoproterozoic collapse of atmospheric methane. *Geobiology* **4**, 271–283.

Zhang F., Romaniello S. J., Algeo T. J., Lau K. V., Clapham M. E., Richoz S., Herrmann A. D., Smith H., Horacek M. and Anbar (2018) Multiple episodes of extensive marine anoxia linked to global warming and continental weathering following the latest Permian mass extinction. *Sci. Adv.* **4**, e1602921.

*Associate editor:* Alexander Nemchin